CELL STRUCTURE AND FUNCTION 33: 109–122 (2008)

Dynein-dependent Movement of Autophagosomes Mediates Efficient Encounters with Lysosomes

Shunsuke Kimura[1], Takeshi Noda[1], and Tamotsu Yoshimori[1,2]*

[1]*Research Institute for Microbial Diseases, Osaka University, Osaka 565-0871, Japan and* [2]*CREST, Japan Science and Technology Agency, Kawaguchi-Saitama 332-0012, Japan*

ABSTRACT. **Autophagy is a membrane trafficking pathway that carries cytosolic components to the lysosome for degradation. During this process, the autophagosome, a double-membraned organelle, is generated *de novo*, sequesters cytoplasmic proteins and organelles, and delivers them to lysosomes. However, the mechanism by which autophagosomes are targeted to lysosomes has not been determined. Here, we observed the real-time behavior of microtubule-associated protein light chain 3 (LC3), which localizes to autophagosomes, and showed that autophagosomes move in a microtubule- and dynein-dynactin motor complex-dependent manner. After formation, autophagosomes show a rapid vectorial movement in the direction of the centrosome, where lysosomes are usually concentrated. Microinjection of antibodies against LC3 inhibited this movement; furthermore, using FRAP, we showed that anti-LC3 antibody injection caused a defect in targeting of autophagosomes to lysosomes. Collectively, our data demonstrate the functional significance of autophagosome movement that enables effective delivery from the cytosol to lysosomes.**

Key words: autophagy/microtubule/dynein/LC3/lysosome

Introduction

Autophagy is an intracellular bulk degradation system in which cytoplasmic components, such as proteins and organelles, are directed to lysosomes by a membrane-mediated process (Seglen and Bohley, 1992; Yoshimori, 2004). During autophagy, a small cisterna, called the isolation membrane, elongates and surrounds a portion of the cytoplasm to form a double-membraned structure, the autophagosome. Eventually, lysosomes fuse with autophagosomes and the sequestered cytoplasmic components are degraded. Autophagy is regulated by nutrient availability and hormones, and may be essential for cellular homeostasis. In addition to its homeostatic function, autophagy plays important physiological roles in intracellular protein quality control under normal conditions (Hara *et al*., 2006; Komatsu *et al*., 2006), and as a defense mechanism against bacterial pathogens (Nakagawa *et al*., 2004; Ogawa *et al*., 2005) or the toxic effects of aggregation-prone proteins (Kamimoto *et al*., 2005; Ravikumar *et al*., 2002).

A series of Atg proteins function in autophagy in yeast; these proteins are conserved throughout eukaryotes (Klionsky and Ohsumi, 1999; Yoshimori, 2004). In mammalian cells, Atg5 is an autophagy-related protein that is localized on isolation membranes and is essential for autophagosome formation (Mizushima *et al*., 2001). Microtubule-associated protein 1 light chain 3 (LC3) is a mammalian homologue of yeast Atg8 (Kabeya *et al*., 2000; Kirisako *et al*., 1999). The C-terminal fragment of LC3 is cleaved by Atg4 to yield a cytosolic form, LC3-I. LC3-I can be modified by phosphatidylethanolamine at its carboxy-terminal glycine residue via a ubiquitination-like reaction (Ichimura *et al*., 2000; Tanida *et al*., 2004). The resulting lipidated form, LC3-II, associates with both the outer and inner membranes of the autophagosome during and after formation (Kabeya *et al*., 2000), and the amount of LC3-II correlates with the extent of autophagosome formation (Kabeya *et al*., 2000). Autophagosomes are thought to be generated *de novo* rather than arising from preexisting organelles such as the ER (Noda *et al*., 2000). The events that occur between generation and eventual fusion with endosomes and/or lysosomes are poorly characterized. Therefore, we analyzed the spatial

*To whom correspondence should be addressed: Tamotsu Yoshimori, Research Institute for Microbial Diseases, Osaka University, Osaka 565-0871, Japan.
Tel: +81–6–6879–8293, Fax: +81–6–6879–8295
E-mail: tamyoshi@biken.osaka-u.ac.jp

Abbreviations: LC3, microtubule-associated protein 1 (MAP1) light chain 3; mRFP, monomeric red fluorescent protein (mRFP); dyneinIC, Dynein intermediate chain; FRAP, Fluorescence Recovery After Photobleaching.

and temporal behavior of both the isolation membrane and autophagosome by following Atg5 and LC3, respectively. By combining real-time observation and microinjection techniques, we describe herein that, after formation, autophagosomes utilize a dynein-microtubule system to rapidly move toward lysosomes located near the centrosome. This is prerequisite for efficient lysosome targeting of autophagosomes, which are generated at points distant to lysosomes.

Materials and Methods

Cell culture, transfection, and plasmids

All cell lines were cultured in DMEM (Sigma) supplemented with 8% heat-inactivated FBS (Gibco). Transfections were performed using LipofectAMINE 2000 (Invitrogen) according to the manufacturer's protocol. For amino acid starvation, cells were cultured in HBSS (Gibco) lacking amino acids and fetal bovine serum for 2 h. Stable transformants were selected in complete medium containing 500 μg/ml G418 (Sigma).

The pEGFP-LC3 (Kabeya *et al*., 2000), mRFP-LC3 (Kimura *et al*., 2007), and GFP-Atg5 (Mizushima *et al*., 1998) plasmids were previously described. FLAG-dynamitin plasmid was a generous gift from Dr. Mitsuo Tagaya (Tokyo University of Pharmacy and Life Science) (Hirose *et al*., 2004).

Antibodies

Mouse monoclonal anti-alpha-tubulin (B5-1-2), anti-cytoplasmic dynein intermediate chain (70.1) (Sigma), control ascites, anti-p150^{Glued} (BD bioscience), anti-lamp1 antibody (H4A3), rabbit anti-gamma-tubulin antibodies (Santa Cruz) are all commercially available. Anti-LC3 antibodies against recombinant full length LC3 (SK2-6) and N-terminal LC3 peptide (N15) were prepared as previously described (Kabeya *et al*., 2000). Anti-LC3 antibody (SK2-6) was purified on an immobilized GST-LC3-glutathione-Sepharose column. Preparation of Fab fragment was performed as previously described (Coulter and Harris, 1983). Immobilized Papain (PIERCE) was used to digest purified anti-LC3 antibody. Protein A-Sepharose CL-4B (Amersham) was used to remove undigested IgG and Fc fragments. Purified Fab fragment was confirmed with SDS-PAGE followed by Coomassie brilliant blue staining.

Immunocytochemistry and fluorescence microscopy

For immunofluorescence microscopy, cells were plated on non-coated 12-mm cover slips and cultured for 24 h. These cells were transferred to Hanks' medium and cultured for 2 h, followed by pre-permeabilization with 50 μg/ml digitonin in PBS for 10 min at room temperature, and fixation in 3% paraformaldehyde in PBS at room temperature. After fixation, the cells were permeabilized with 50 μg/ml digitonin in PBS for 5 min at room temperature. The cells were stained with anti-alpha-tubulin antibody (1:400 dilution), anti-cytoplasmic dynein antibody (1:100) or anti-p150^{Glued} antibody (1:100) and affinity purified anti-LC3 antibody (1:100) for 1 h at room temperature. After appropriate secondary antibody treatment, samples were examined under a fluorescence laser scanning confocal microscope (FV1000, Olympus).

Time-lapse microscopy

For live cell imaging, cells were seeded on a non-coated 35-mm glass-base dish (Matsunami Glass) one day before use. The cells were observed on a stage equipped with a thermostatically controlled MI-IBC culture dish system at 37°C in 5% CO_2 (Olympus). Images were acquired using an Olympus IX81 microscope with a 100 × immersion objective lens (N.A. 1.35) equipped with a mercury lamp and cooled charge-coupled device camera (Roper Cool Snap HQ), under control of Slide Book software (Intelligent Imaging Innovations Inc., Denver, CO). Images were deconvoluted and normalized with Slide Book software. Trajectory, maximum speed and total displacement analyses were performed using ImageJ software (http://rsb.info.nih.gov/ij/).

Correlative analysis of live cell imaging and immunocytochemistry

Live cell imaging was performed as above. Cells were cultured on a non-coated glass-base culture dish with grid lines (MatTek). After live cell imaging, cells were fixed with ice-cold methanol for 30 sec, stained with anti-lamp1 antibody (1:100) and anti-gamma-tubulin antibody (1:100) as above, and stained with secondary antibody. The field observed by time-lapse microscopy was identified by grid line and images were superimposed using Photoshop CS (Adobe).

Microinjection

Microinjection was performed at 37°C using a semiautomatic Eppendorf Microinjection system and an IX81 fluorescence microscope (Olympus) equipped with an MI-IBC culture dish system (Olympus) for temperature control as described above. The antibodies for microinjection were diluted in PBS, and aliquots were centrifuged at 15,000 rpm for 15 min at 4°C before microinjection. Prior to microinjection, cells were subjected to starvation for 60 min, and were then injected under the following conditions: antibody concentration of 0.4 mg/ml in PBS, with an injection pressure of 30 hPa, and an injection time of 0.4 sec. For antibody-antigen competition, recombinant LC3 protein or N-terminal peptide was included in the microinjection experiments. The injected cells were incubated for 30 min on stage at 37°C with 5% CO_2, and then observed by time-lapse microscopy.

Fluorescence Recovery After Photobleaching (FRAP)

For FRAP assays, cells stably expressing mRFP-LC3 were seeded on a non-coated 35-mm glass-base dish (Matsunami Glass) and

incubated with 0.5 mg/ml of Alexa488-BSA overnight to mark lysosomes. The cells were transferred to new culture medium and incubated for 4 h. Cells were then subjected to starvation in Hanks' solution and observed using an FV1000 confocal microscopy system (Olympus) utilizing a Plan-Apo 100×1.35 numerical aperture (N.A.) oil differential interference (DIC) lens at 3× digital zoom on a thermostatically controlled stage heater (MATS55-RAF20, Tokai). The perinuclear region was photobleached using a 543-nm HeNe laser at 100% power for 0.5 sec (3 times). Pre-bleach and post-bleach images were observed by time-lapse microscopy. For time-lapse microscopy, Alexa488 was excited with the 488-nm line of a 30 mW argon laser at 1% power. mRFP was excited with the 543-nm line of a 1 mW HeNe laser at 15% power. Images were collected at 512×512 pixel resolution, 2 μm/sec scan speed and 30 sec intervals.

Results

Autophagosome formation takes place throughout the cytoplasm

Atg5 protein binds to isolation membranes during autophagosome formation and is detached when formation is completed (Mizushima *et al*., 2001). Therefore, GFP-Atg5 can be used to monitor autophagosome formation. Using HeLa cells stably expressing GFP-Atg5, we first asked whether autophagosome formation takes place in a specialized area within the cell.

We observed punctate GFP-Atg5 signals throughout the cytoplasm (Fig. 1A). This is in contrast to the lysosome marker lamp1, which primarily localized around the centrosome (Fig. 1A); this clustered localization pattern of lysosomes is common in various cell lines (Aumuller *et al*., 1997; Burkhardt *et al*., 1997; Dunster *et al*., 2002; Matteoni and Kreis, 1987). Measurement of the distance from the centrosome showed a sharp peak in the distribution of

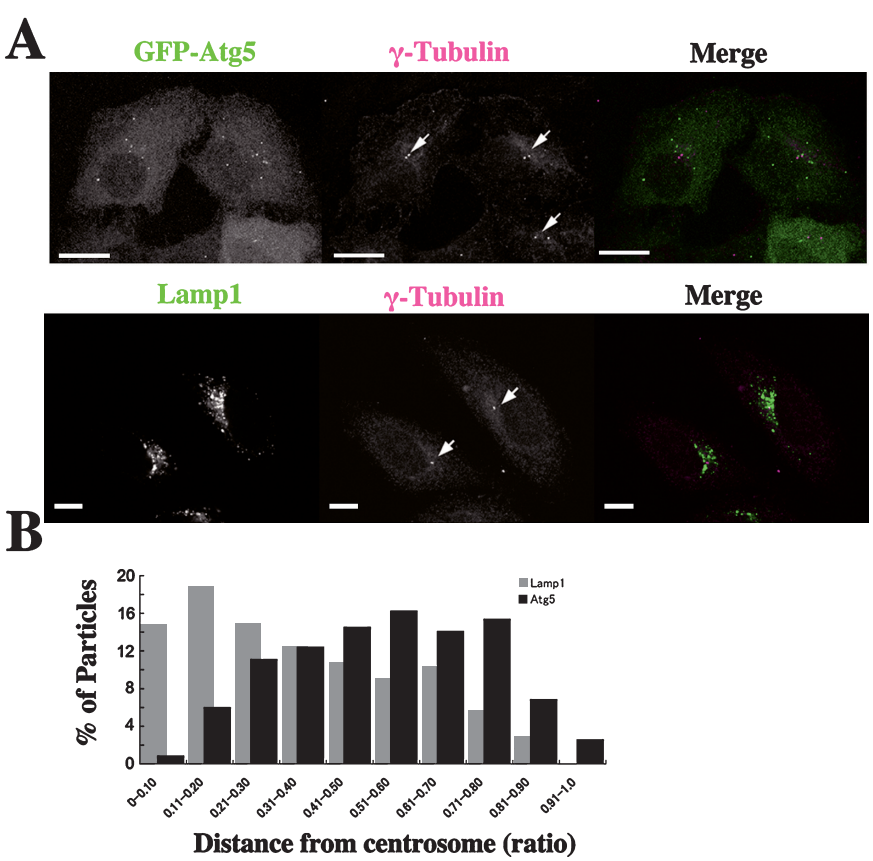

Fig. 1. GFP-Atg5 distribution within a cell. (A) HeLa cells expressing GFP-Atg5 were observed, fixed, and stained for gamma tubulin and Lamp1. Images of live and fixed cells were superimposed according to grid line. GFP-Atg5 and gamma-tubulin (upper panel), or Lamp1 and gamma-tubulin (lower panel) are shown. Gamma-tubulin is indicated by arrows. The bar indicates 10 μm. (B) Distances were measured using ImageJ software and are presented as ratios of the distance between the centrosome and autophagosome or lysosome relative to the distance from the centrosome to the plasma membrane. More than 100 dots were measured and the data are depicted in a histogram.

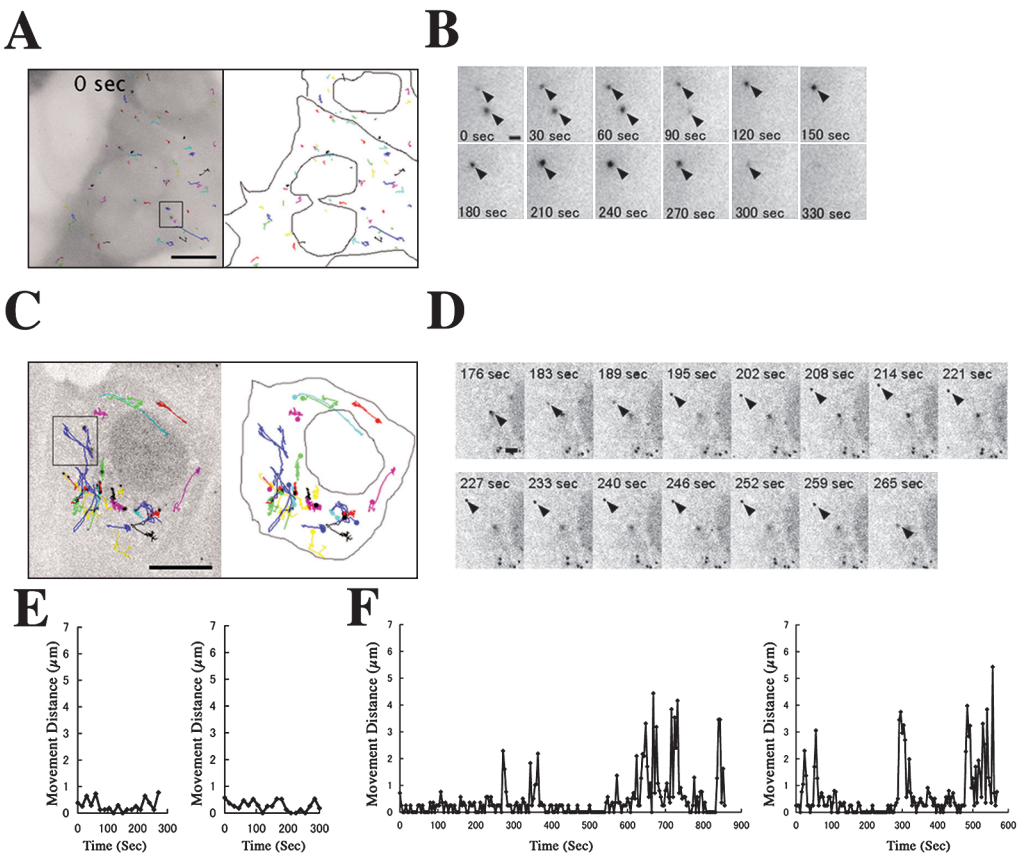

Fig. 2. Real time observation and trajectory analysis of GFP-Atg5 and GFP-LC3 dynamics. Time-lapse analysis of HeLa cells stably expressing GFP-Atg5 or GFP-LC3 was performed as described in the Materials and Methods. Trajectory analysis of autophagosomes was performed using ImageJ software. (A and C) Representative examples of trajectories of GFP-Atg5 (A) or GFP-LC3 (C) puncta are shown. The image is inverted grey scale acquired by time-lapse microscopy. Black dots indicate GFP signals. Trajectories of GFP-Atg5 (A) or GFP-LC3 (C) are shown by colored lines. Outlines of the cell and nucleus are depicted as continuous lines from a phase contrast image taken at the beginning of the time-lapse sequence. The bar indicates 10 μm. (B and D) High magnification images of selected regions from panels A and C are shown in B and D, respectively. The bar indicates 1 μm. (E and F) Examples of particle distance moved are shown. Each distance was plotted at the time-lapse interval. Two typical examples of GFP-Atg5 (E) or GFP-LC3 (F) particles are shown.

lamp1 signal in the vicinity of the center of the cell; in contrast, the distribution of GFP-Atg5 signal was rather broad (Fig. 1B). These results imply that a large number of autophagosomes form at a distance from the lysosomes, and raised the question of the mechanism by which autophagosomes are delivered to lysosomes.

Autophagosomes move toward the cell center

We extended this analysis by using time-lapse microscopy and followed the dynamics of GFP-Atg5 or GFP-LC3 expressed stably in HeLa cells. Over a period of 15 min, each signal was traced for each frame for a 2-sec interval. After its appearance, the GFP-Atg5 signal did not move extensively and disappeared after 279±56 sec (an average of 15 particles and ±SD, Fig. 2, A, B, and E). This lifetime is different from that observed in mouse embryonic stem cells (9.7±1.8 min) (Mizushima *et al*., 2001). This discrepancy is most likely due to differences in cell lines and observation conditions, such as a temperature control system. In contrast to GFP-Atg5 signals, GFP-LC3 showed a longer life-span and dynamic movement (Fig. 2, C and D). Further, GFP-LC3 puncta moved in a bimodal manner: slow motion (<1 μm/sec) and rapid vectorial movement (>1 μm/sec) (Fig. 2F). In general, after a 3- to 10-min period of slow motion, GFP-LC3 started rapid movement.

We next investigated the directionality of GFP-LC3 movement. Following time-lapse observations, the centrosome was stained as the cell center using anti-gamma-tubulin antibody, and a trajectory image of autophagosome movement was superimposed on it (Fig. 3, A and B). The distance between each GFP-LC3 dot and the centrosome was measured for each frame and the difference from the previous frame was presented. Negative values indicate a

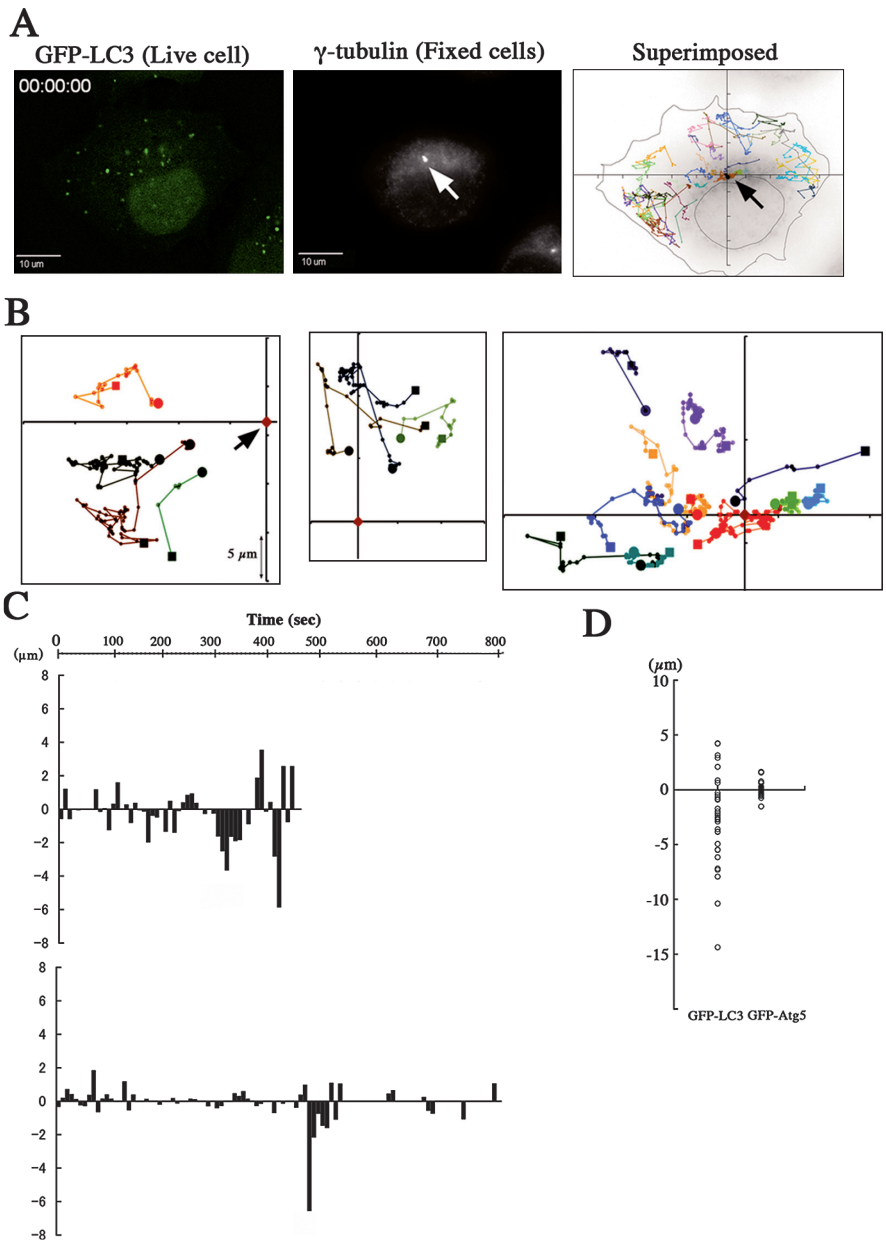

Fig. 3. Assessment of direction of GFP-LC3 movement. (A) Time-lapse imaging of HeLa cells stably expressing GFP-LC3 was performed as described. Cells were then fixed and stained for gamma-tubulin. Trajectory analysis of GFP-LC3 puncta was performed as described in the Materials and Methods. Arrows show gamma-tubulin. (B) Examples of trajectory paths of GFP-LC3 puncta are shown. The center of the axis is the centrosome (red rhomboid). The vertical and horizontal scales are 5 μm. Squares show start points and circles show end points of the trajectory paths. (C) Differences between frames are presented for representative dots. (D) Distances between GFP-LC3 dots and the centrosome at the start point and end point were calculated by ImageJ software. Negative values indicate displacement toward the centrosome.

dot that has moved closer to the centrosome between frames (Fig. 3C). We observed prominent consecutive rapid movements in the direction of the centrosome lasting for over 10 sec (Fig. 3C). However, we also observed rapid movements away from the centrosome, though these occurred less frequently and lasted for shorter periods (Fig. 3C). Distances between GFP-LC3 dots and the centrosome at the start (the start of observation or appearance of dots) and end point (the end of observation or disappearance of dots) were also measured. A trend of most of the dots moving closer to the centrosome was apparent (Fig. 3D).

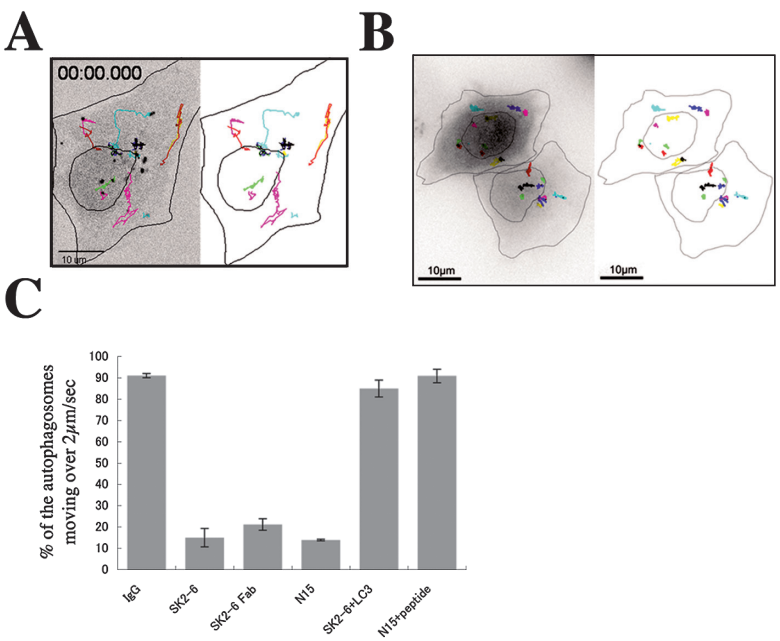

Fig. 4. Effects of anti-LC3 antibody microinjection on autophagosome movement. HeLa cells stably expressing GFP-LC3 were injected with either normal rabbit IgG (A) or affinity purified anti-LC3 antibody (SK2-6) (B). After injection, cells were observed by time-lapse microscopy as described in the Materials and Methods. GFP-LC3 paths are shown by colored lines. The outlines of the cell and nucleus are represented as continuous lines from a phase contrast image taken at the beginning of the time-lapse sequence. The bar indicates 10 μm. (C) A quantitative summary of the inhibition of autophagosome movement by microinjection of anti-LC3 antibodies is shown. The maximal speed of each puncta was measured by ImageJ software. IgG: normal rabbit IgG, SK2-6: affinity purified anti-LC3 antibody, SK2-6 fab: Fab fragment of affinity purified anti-LC3 antibody, N15: affinity purified antibody against N-terminal peptide of LC3, SK2-6+LC3: SK2-6 with recombinant LC3 protein, N15+peptide: N15 with N-terminal LC3. At least 50 fluorescent particles were tracked. The columns show the percentage of autophagosomes moving over 2 μm/sec.

Anti-LC3 antibody microinjection inhibits autophagosome movement

It is possible that the centrosome-directed movement of autophagosomes is required for their efficient targeting to perinuclear-clustered lysosomes. To substantiate this hypothesis, we next sought conditions that would interrupt the rapid autophagosome movement. In agreement with previous reports (Fass *et al*., 2006; Kochl, 2006), we showed that autophagosome movement depends on microtubules, as detailed below. Unfortunately, disruption of the microtubule network by drugs such as nocodazole cannot be used to analyze targeting, since this drug also perturbs lysosomal distribution. Therefore, we tested the effect of microinjection of antibodies against LC3, which is known to possess microtubule binding activity via its N-terminal domain (Kouno *et al*., 2005). HeLa cells stably expressing GFP-LC3 were transferred to starvation medium for 60 min to induce autophagosome formation, and were then microinjected with several antibodies and followed by time-lapse microscopy. As shown above, after a 5-min formation period associated with GFP-Atg5, GFP-LC3 positive autophagosomes transitioned from a slow movement mode to a rapid movement mode. Antibody microinjection might have an effect on this movement that would allow analysis of the dynamics of the autophagosome following formation. Indeed, injection of control IgG had no effect on autophagosome movements (Fig. 4A), whereas injection of affinity-purified anti-LC3 antibodies strongly inhibited rapid movements (Fig. 4, B and C). To minimize the secondary effects of antibody crosslinking, we also injected an Fab fragment of the anti-LC3 antibody, and obtained similar results (Fig. 4C). Furthermore, antibodies raised against the N-terminal peptide (residues 1–15) of LC3 also inhibited rapid movement (Fig. 4C). In contrast, microinjection of anti-LC3 antibody with an excess amount of antigen did not alter movement, indicating that the effect of the injected antibodies is due to antigen-antibody specific interactions (Fig. 4C). As shown in Figure S1, the microinjection of antibodies against LC3 did not disrupt microtubule organization.

Autophagosome movement is important for the targeting to lysosome

Next, we attempted to analyze the correlation between autophagosome movements and the delivery of autophagosomes to lysosomes. For this purpose, we utilized the

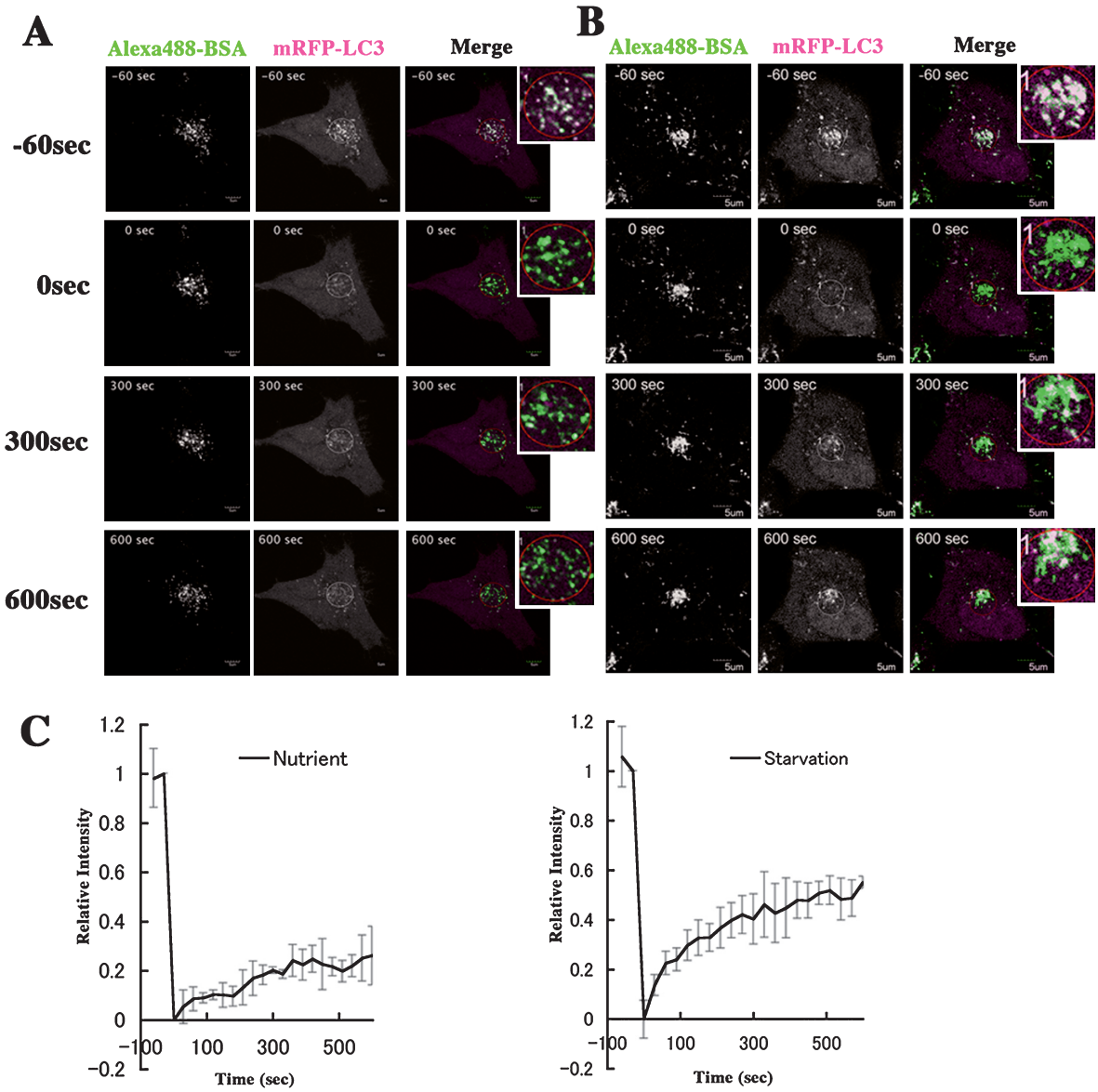

Fig. 5. FRAP analysis of autophagosome movement. (A and B) A representative sequence of images from a FRAP experiment. HeLa cells stably expressing mRFP-LC3 were cultured in nutrient rich medium (A) or transferred to Hanks' solution for 60 min for starvation (B). The cells are shown in the upper panel prior to photobleaching (–60 sec). The region marked by a circle was photobleached at time zero as described in the Materials and Methods, and fluorescent intensity was monitored. Insets are high magnification images around the circled area. (C) The change of fluorescence intensity in the bleached area was plotted. The value zero was defined as the value obtained soon after photobleaching. The relative intensity was defined as the ratio of the intensity at each time point to the pre-bleach intensity (–30 sec). Values indicate averages and SDs of three independent experiments.

fluorescence recovery after photobleaching (FRAP) technique (Jordens *et al*., 2001) with a monomeric red-fluorescence protein-LC3 fusion, which is delivered to lysosomes along with sequestered cytoplasmic components (Kabeya *et al*., 2000; Kimura *et al*., 2007). We have previously reported that, in contrast to GFP-LC3, mRFP-LC3 can label autolysosomes, the fusion product of autophagosomes and lysosomes, due to its stability under the conditions within the lysosome (Kimura *et al*., 2007). When the fusion of autophagosomes and lysosomes was abrogated by overexpression of dominant negative Rab7, mRFP-LC3 no longer colocalized with lysosomal markers, indicating that colocalization resulted from autolysosome formation (Kimura *et al*., 2007).

In cells stably expressing mRFP-LC3, numerous mRFP-LC3 puncta were observed even in the presence of nutrients, when autophagy is not induced (Fig. 5A). We interpret this as constitutive baseline autophagy, which occurs during

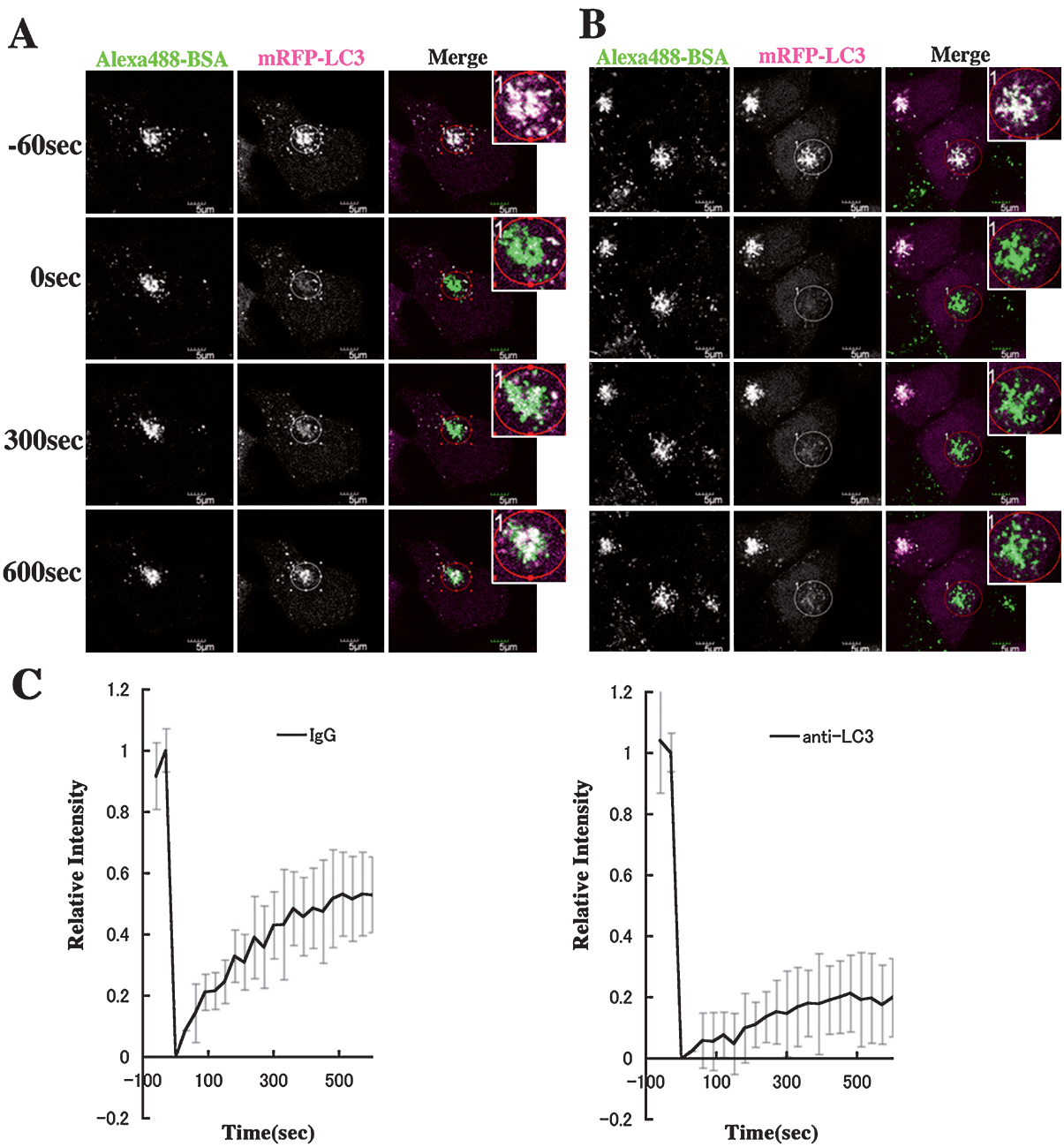

Fig. 6. Microinjection of anti-LC3 antibody and FRAP analysis. (A and B) A representative sequence of images from a FRAP experiment. HeLa cells stably expressing mRFP-LC3 cultured under starvation condition and injected with control IgG (A) or anti-LC3 antibody (B). A region of the prebleached cell is shown in the upper left panel, followed by an image showing a region marked by a circle, which was photobleached at time zero. Fluorescence intensity was monitored over time. Insets are high magnification images around the circled area. (C) The change of fluorescence intensity in the bleached area was plotted. The value zero was defined as the value obtained soon after photobleaching. The relative intensity was defined as the ratio of the intensity at each time point to the pre-bleach intensity (–30 sec). Values indicate averages and SDs of three independent experiments.

propagation of the cells, because this signal is not observed in Atg5 deficient cells (Kimura *et al*., 2007). These puncta colocalized with lysosomes marked by Alexa488-BSA incorporated via endocytosis (Fig. 5A) (Kimura *et al*., 2007). The colocalization was accumulated near the centrosome (87±7.0%, within the circled area in Fig. 5, A and B), and this clustered localization pattern allowed selective photobleaching. Moreover, mRFP-LC3 signals in this region are higher than that localized on autophagosomes due to their concentration within the lysosomes probably as

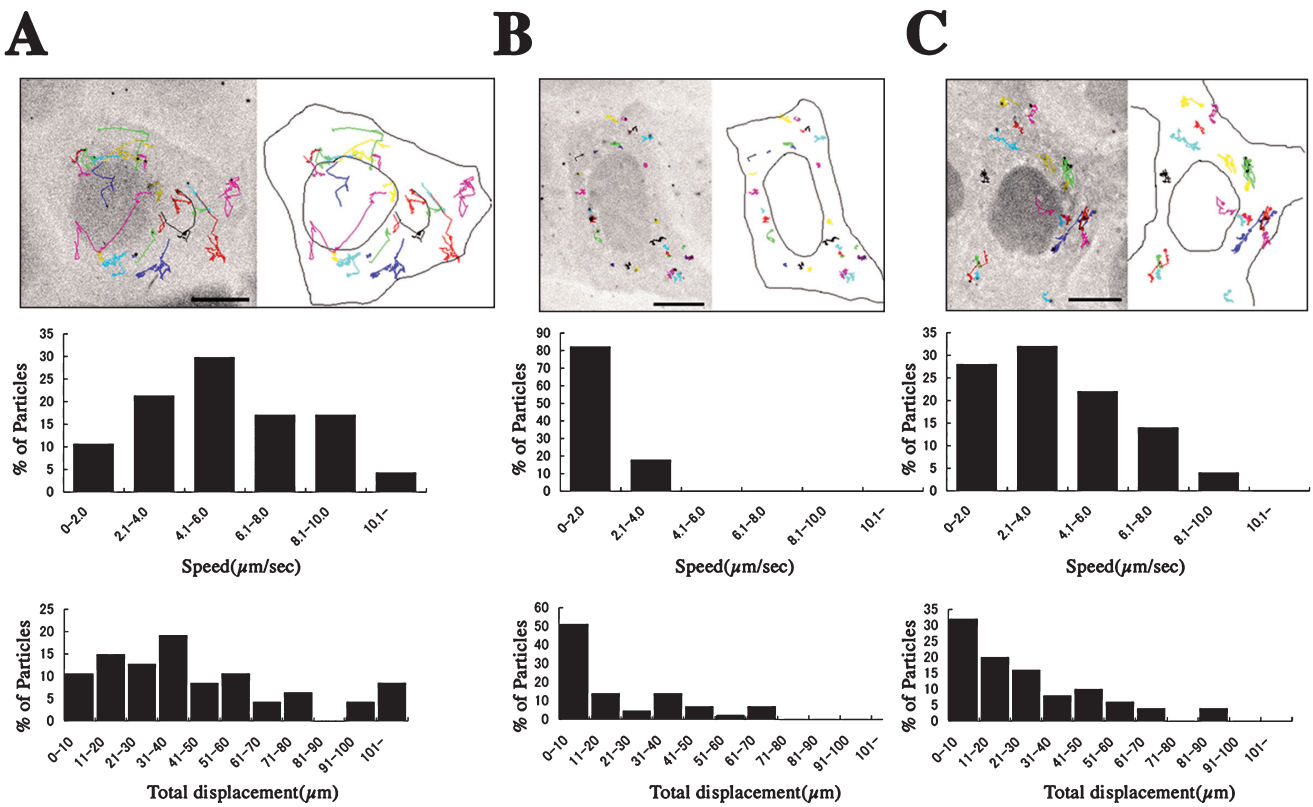

Fig. 7. Effects of nocodazole and taxol on autophagosome movement. HeLa cells stably expressing GFP-LC3 were treated with DMSO as a control (A), 25 μM nocodazole (B), or 10 μM Taxol (C). Time-lapse analysis was performed as described in Materials and Methods. Trajectory analysis of autophagosomes was performed using ImageJ software. Representative examples of trajectories of GFP-LC3 puncta in the cells are shown. The image is inverted grey scale acquired from time-lapse microscopy. Black dots indicate GFP signals. Trajectory paths of GFP-LC3 puncta are shown by colored lines. The outlines of the cell and nucleus are depicted as continuous lines from a phase contrast image taken at the beginning of the time-lapse sequence. The bar indicates 10 μm. Histograms show the distribution of maximum speeds (middle) and the distribution of total displacements (bottom) for a period of time of 10 min. At least 50 fluorescent particles were tracked. The number of fluorescent particles with a given maximum speed or total displacement is calculated as a percentage of the total number of analyzed fluorescent particles.

a result of multiple fusions of autophagosomes. This concentrated signal made it easy to monitor the changes in the efficiency of mRFP-LC3 delivery to lysosomes. After bleaching of mRFP fluorescence in this region, the recovery of the fluorescent signal was measured. In the presence of nutrients, the recovery of mRFP-LC3 signal was 26±11% at 10 min after bleaching (Fig. 5, A and C). mRFP fluorescence was recovered more rapidly under starvation conditions (55±2% at 10 min) (Fig. 5, B and C). In our experiment, the localization pattern of lysosomes was not significantly changed by starvation (Fig. 5, A and B), suggesting that difference of the recovery rate of mRFP in the FRAP assay is not due to the effects of starvation on lysosomes, but represents starvation-induced autophagic activity.

Using this FRAP assay, the effect of abrogating the movement of autophagosomes was assessed. Injection of control IgG had no effect on the recovery of mRFP-LC3 signal in the perinuclear region (Fig. 6, A and C). In contrast, when autophagosome movement was inhibited by microinjection of anti-LC3 antibody, the recovery of mRFP-LC3 signal was severely impaired (Fig. 6, B and C). As shown in Figure S2, injection of LC3 antibody did not significantly affect the number of autophagosomes induced by starvation (Fig. S2). These results indicate that the rapid movement is prerequisite for autophagosome delivery to lysosomes.

Dynein-dynactin dependent autophagosome movement

Our trajectory analysis showed that most consecutive rapid autophagosome movements were aligned in the same direction (Fig. 3). This linear motion suggests the possibility that rails exist for rapid autophagosome movement. While this study was underway, two reports demonstrated that autophagosomes move in a microtubule-dependent manner (Fass *et al*., 2006; Kochl, 2006). Consistent with these reports, we found that the maximal speed of movement was decreased by treatment with nocodazole, a microtubule depolymeriz-

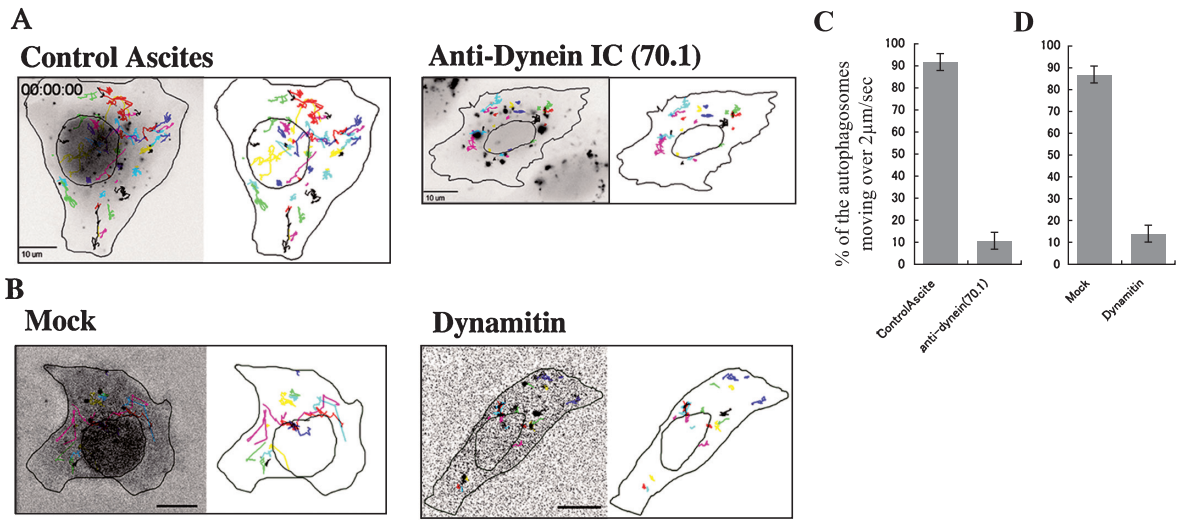

Fig. 8. Effects of abrogation of dynein function. (A) HeLa cells stably expressing GFP-LC3 were microinjected with control ascites (left panel), or anti-dynein IC antibody (clone 70.1) (right panel). Time-lapse analysis was performed as described in the Materials and Methods. (B) HeLa cells stably expressing GFP-LC3 were transfected with mock vector and mRFP (left panel), or FLAG-dynamitin and mRFP expression vectors (right panel). After 36–48 h, time-lapse analysis was performed as described in the Materials and Methods. GFP-LC3 paths are shown by colored lines. The outlines of the cell and nucleus are represented as continuous lines from a phase contrast image taken at the beginning of the time-lapse sequence. The bar indicates 10 μm. (C and D) Quantitative summary of inhibition of autophagosome movement following microinjection of anti-dynein antibodies (C) or overexpression of dynamitin (D). The maximal speeds of the puncta were measured using ImageJ software. At least 50 fluorescent particles were tracked. The columns show the percentage of autophagosomes moving over 2 μm/sec.

ing agent (Fig. 7). In untreated cells, the maximum movement was 5.3±2.6 μm/sec (Fig. 7A); in nocodazole-treated cells, movement was 1.0±0.8 μm/sec (Fig. 7B). Nocodazole eliminated both long-range and linear motions (Fig. 7B). Treatment also decreased the number of autophagosomes that moved over 11 μm, and increased the number that moved less than 10 μm (Fig. 7B). The average total displacement was 48±38 μm in untreated cells, whereas it was 10±9 μm in the nocodazole-treated cells. We next examined whether microtubule depolymerization is involved in this movement, as has been reported in the case of chromosome movement (Coue *et al*., 1991; Inoue and Salmon, 1995). We treated cells with taxol, a microtubule stabilizing regent, and found that this decreased the maximal speed of movement (3.7±2.3 μm/sec) and long-range motion (25±22 μm), although these effects were not as dramatic as those of nocodazole (Fig. 7C). In addition, trajectory analysis showed that linear motion remained in the taxol-treated cells (Fig. 7C). Therefore, depolymerization may not provide the primary force for movement.

Dynein is a motor protein that moves toward the minus end of microtubules (Gill *et al*., 1991; Schroer and Sheetz, 1991). Dynein interacts with its partner dynactin to form a large complex, which is essential for motor activity. Although it has been reported that abrogating dynein function leads to defective clearance of aggregated proteins by autophagy (Ravikumar *et al*., 2005), it is unclear how dynein is involved in this process. To analyze the involvement of the dynein-dynactin complex in autophagosome movement, we attempted to inhibit the function of the motor protein. Microinjection of anti-dynein intermediate chain (clone 70.1) antibody, which is known to impair dynein activity (Burkhardt *et al*., 1997; Heald *et al*., 1996; Nielsen *et al*., 1999), almost completely impaired the rapid autophagosome movements (Fig. 8, A right and C), while control ascites had little effect (Fig. 8, A left and C). We next overexpressed dynamitin, a subunit of the dynein-dynactin complex (Echeverri *et al*., 1996); this is known to inhibit dynein- and dynactin-dependent organelle movement (Burkhardt *et al*., 1997). HeLa cells stably expressing GFP-LC3 were co-transfected with a FLAG-dynamitin expression vector along with an mRFP expression vector as a transfection marker. As shown in Fig. 8, B and D, autophagosome movements were significantly reduced in cells expressing FLAG-dynamitin (Fig. 8, B right and D). Movements were unaffected in control cells expressing mRFP alone (Fig. 8, B left and D). We next performed immunocytochemistry on these molecules. LC3 labeled autophagosomes were arranged along microtubule tracts (Fig. 9A). In addition, a subset of endogenous LC3 puncta colocalized with dynein intermediate chain and p150^{glued}, another subunit of the dynactin complex (Holzbaur *et al*., 1991) (Fig. 9, B and C). Taken together, these data indicate that the dynein-dynactin complex is involved in autophagosome movement.

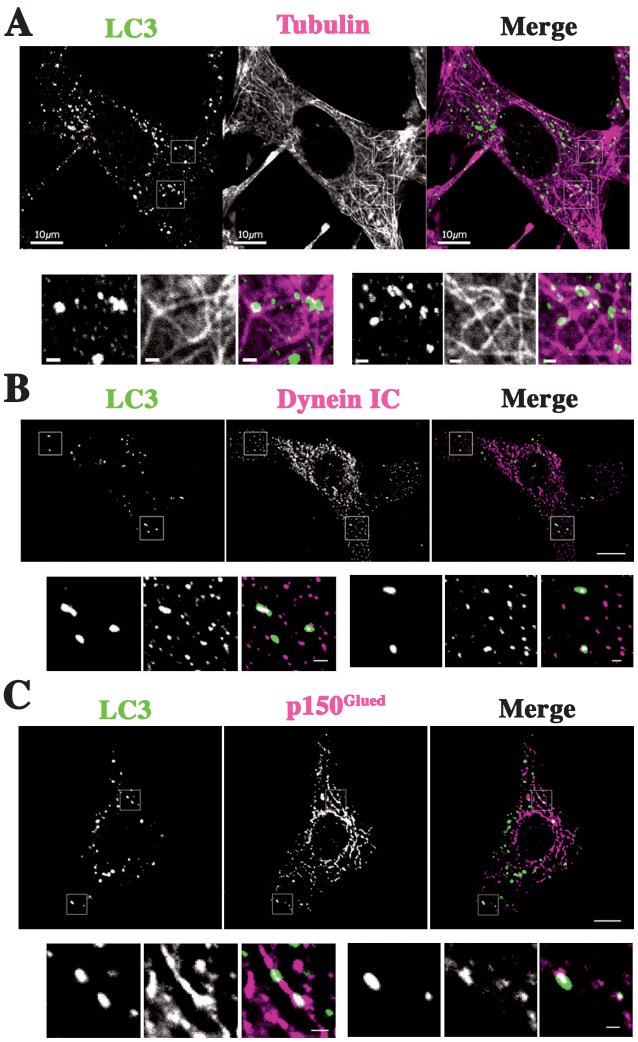

Fig. 9. Immunocytochemistry of endogenous LC3 with dynein-dynactin or microtubules. (A) MEF cells were fixed and stained for LC3 (SK2-6) and alpha-tubulin. Bars indicate 10 μm. Lower panels are high-magnification views of the boxed areas in the upper panels. Bars indicate 1 μm. (B and C) MEF cells were stained for LC3 (SK2-6 AP) and intermediate chain (clone 70.1) (B) or dynein and $p150^{glued}$ (C). Bars indicate 10 μm. Lower panels are high-magnification views of the boxed areas in the upper panels. Bars indicate 1 μm.

Discussion

In this report, we have described the spatial and temporal itinerary of autophagosomes by tracing the dynamics of two marker proteins, Atg5 and LC3, with live imaging techniques. The initiation of autophagosome formation remains a fundamental question in the study of autophagy. In the case of yeast, the pre-autophagosomal structure (PAS) is proposed as the site of autophagosome formation (Suzuki *et al*., 2002). Many of the Atg proteins accumulate at the PAS, and interestingly, the PAS is adjacent to the vacuole, equivalent to the mammalian lysosome (Suzuki *et al*., 2002; Suzuki *et al*., 2007). In the case of mammalian cells, the earliest structure identified during autophagosome formation is crescent-like and positive for Atg5, but little else about it is known (Mizushima *et al*., 2001). Here, we have shown that, in mammalian cells, autophagosomes form throughout the cytoplasm. Using time-lapse microscopy, we have also shown that autophagosomes or their precursors, isolation membranes, do not move far from their formation site until they are fully formed. After completion, autophagosomes exhibit rapid vectorial movement that generally tends to be in the direction of lysosomes located near the centrosome.

Molecular insight into autophagosome dynamics

In mammalian cells, a number of reports have shown that microtubule inhibitors interfere with degradation by autophagy and the fusion of autophagosomes with lysosomes (Aplin *et al*., 1992; Blankson *et al*., 1995; Fengsrud *et al*., 1995; Iwata *et al*., 2005; Kochl, 2006; Ravikumar *et al*., 2005; Webb *et al*., 2004). However, these reports are somewhat inconsistent, with some suggesting that microtubules are involved in autophagosome formation (Kochl, 2006), and some reporting little effect on lysosomal targeting (Fass *et al*., 2006). We now provide novel and more direct evidence that microtubules and the dynein motor complex are involved in the autophagic process. In particular, we show that perturbation of dynein function impairs rapid autophagosome movement. Although it remains possible that this is a secondary effect, we favor the possibility that dynein is the motor for autophagosome movement based on the following results. First, the average velocity of rapid autophagosome movement described in this study (5 μm/sec) is coincident with that reported for the dynein motor (4 μm/sec) (Lakadamyali *et al*., 2003). Second, microinjection and real time observation reduce the possibility of secondary effects that are occasionally seen in transfection experiments. Third, GFP-LC3 and dynein partially co-localize. This seems quite reasonable, as dynein is also involved in other trafficking events (Aniento *et al*., 1993; Burkhardt *et al*., 1997; Harada *et al*., 1998), and nascent GFP-LC3 positive autophagosomes may not yet have acquired dynein molecules. The mechanisms by which dynein may be recruited to autophagosomes are completely unknown. One possibility is that dynein is directly or indirectly associated with LC3. Supporting a role for LC3 in the process of autophagosome movement, we showed that microinjection of antibody against LC3 impaired rapid movement. The identification of a putative dynein anchor protein is an important issue to be pursued. During our observations, we observed a transition from a slow motion phase to a rapid movement phase. Recruitment of a motor may be one possible trigger for this transition. Another potential trigger might be a physical interaction between LC3 and micro-

tubules. In the 3-dimensional structure of LC3, in addition to a typical ubiquitin-fold, there is an N-terminal extension consisting of two-alpha-helices (Kouno *et al*., 2005; Sugawara *et al*., 2004), which bind to microtubules (Kouno *et al*., 2005). Here, we showed that microinjection of anti N-terminal LC3 antibody abolished autophagosome movement. Although we cannot exclude the possibility that these antibodies affect the function of other components required for movement by steric hindrance, it seems likely that LC3 plays a role in recruitment of the dynein motor to autophagosomes, recruitment of autophagosomes to microtubules, or both. We note that it is unlikely that we could observe this function of LC3 using knockdown techniques, as LC3 is thought to play a crucial role in autophagosome formation.

Significance of the rapid vectorial movement for autophagy

There remains a discrepancy in the interpretation of the importance of rapid movement between this report and recent reports. In the one report by Fass *et al*., they used nocodazole to disrupt microtubules and showed that the overall rate of autophagosome and lysosome fusion was not affected (Fass *et al*., 2006). In the other report by Jahreiss *et al*., they showed the importance of rapid movement of autophagosome in the fusion with lysosomes by using dynein knockdown (Jahreiss *et al*., 2008). However, nocodazole treatment and disruption of dynein function by RNAi also disturb lysosome distribution and there remains a question in terms of the targeting efficiency under such abnormal conditions (Burkhardt *et al*., 1997). To circumvent this problem, we used other strategies. First, we sought conditions that did not interfere with lysosome distribution, but affected autophagosome movement; microinjection of anti-LC3 antibody met these criteria. Atg8, a yeast homolog of LC3, is required for autophagosome formation (Nakatogawa *et al*., 2007). Even if the anti-LC3 antibody affected autophagosome formation, we would still be able to observe LC3 positive autophagosomes which had already formed at the time of microinjection (Fig. S2). Second, we established a FRAP assay to assess delivery efficiency more directly. Our results showed that rapid movement is essential for efficient targeting of autophagosomes to lysosomes. This seems reasonable because autophagosome formation takes place throughout the cytoplasm while lysosomes are clustered in the cell center (Fig. 1).

What confuses the situation is that the disruption of microtubules and lysosome localization does not profoundly affect the targeting efficiency of the autophagosomes (Fass *et al*., 2006). Random Brownian movement of lysosomes and autophagosomes in the cytoplasm may offer a reasonable efficiency of fusion, or there might be an additional unknown targeting mechanism. Nevertheless, we have demonstrated the importance of the microtubule-based targeting system in a more physiological situation in which lysosomes are clustered in the cell center. Thus, autophagosomes can capture degradation substrates anywhere in the cytoplasm and transport them to lysosomes.

In neuronal cells, autophagosomes formed at the distal end of the axon undergo retrograde transport back to the cell body (Hollenbeck, 1993; Yue, 2007). In these highly elongated cells, dynein- and microtubule-dependent movement of autophagosomes may be more critical to the autophagic process than in other cell types. A recent study has shown that loss of dynein function impairs the autophagic clearance of aggregation-prone proteins; such proteins may be a cause of certain neurodegenerative diseases (Ravikumar *et al*., 2005; Rubinsztein *et al*., 2005). We speculate that autophagy and the dynein-dependent movement of autophagosomes play physiologically important roles in protecting cells against neurodegeneration.

Acknowledgements. We are grateful to Dr. Mitsuo Tagaya (Tokyo University of Pharmacy and Life Science) for FLAG-dynamitin plasmid, Dr. Roger Y. Tsien (University of California, San Diego, USA) for the mRFP1 cDNA, and Dr. Hitomi Yamaguchi (Pharmaceuticals and Medical Devices Agency, Japan) for HeLa cells stably expressing GFP-Atg5. This work was supported in part by the Special Coordination Fund for Promoting Science and Technology of the Ministry of Education, Culture, Sports, Science and Technology (MEXT), and the Naito Foundation.

References

Aniento, F., Emans, N., Griffiths, G., and Gruenberg, J. 1993. Cytoplasmic dynein-dependent vesicular transport from early to late endosomes. *J. Cell Biol*., **123**: 1373–1387.

Aplin, A., Jasionowski, T., Tuttle, D.L., Lenk, S.E., and Dunn, W.A. Jr. 1992. Cytoskeletal elements are required for the formation and maturation of autophagic vacuoles. *J. Cell Physiol*., **152**: 458–466.

Aumuller, G., Renneberg, H., and Hasilik, A. 1997. Distribution and subcellular localization of a lysosome-associated protein in human genital organs. *Cell Tissue Res*., **287**: 335–342.

Blankson, H., Holen, I., and Seglen, P.O. 1995. Disruption of the cytokeratin cytoskeleton and inhibition of hepatocytic autophagy by okadaic acid. *Exp. Cell Res*., **218**: 522–530.

Burkhardt, J.K., Echeverri, C.J., Nilsson, T., and Vallee, R.B. 1997. Overexpression of the dynamitin (p50) subunit of the dynactin complex disrupts dynein-dependent maintenance of membrane organelle distribution. *J. Cell Biol*., **139**: 469–484.

Coue, M., Lombillo, V.A., and McIntosh, J.R. 1991. Microtubule depolymerization promotes particle and chromosome movement in vitro. *J. Cell Biol*., **112**: 1165–1175.

Coulter, A. and Harris, R. 1983. Simplified preparation of rabbit Fab fragments. *J. Immunol. Methods*, **59**: 199–203.

Dunster, K., Toh, B.H., and Sentry, J.W. 2002. Early endosomes, late endosomes, and lysosomes display distinct partitioning strategies of inheritance with similarities to Golgi-derived membranes. *Eur. J. Cell Biol*., **81**: 117–124.

Echeverri, C.J., Paschal, B.M., Vaughan, K.T., and Vallee, R.B. 1996. Molecular characterization of the 50-kD subunit of dynactin reveals function for the complex in chromosome alignment and spindle organization during mitosis. *J. Cell Biol*., **132**: 617–633.

Fass, E., Shvets, E., Degani, I., Hirschberg, K., and Elazar, Z. 2006. Microtubules support production of starvation-induced autophagosomes but not their targeting and fusion with lysosomes. *J. Biol. Chem*., **281**: 36303–36316.

Fengsrud, M., Roos, N., Berg, T., Liou, W., Slot, J.W., and Seglen, P.O. 1995. Ultrastructural and immunocytochemical characterization of autophagic vacuoles in isolated hepatocytes: effects of vinblastine and asparagine on vacuole distributions. *Exp. Cell Res*., **221**: 504–519.

Gill, S.R., Schroer, T.A., Szilak, E., Steuer, E.R., Sheetz, M.P., and Cleveland, D.W. 1991. Dynactin, a conserved, ubiquitously expressed component of an activator of vesicle motility mediated by cytoplasmic dynein. *J. Cell Biol*., **115**: 1639–1650.

Hara, T., Nakamura, K., Matsui, M., Yamamoto, A., Nakahara, Y., Suzuki-Migishima, R., Yokoyama, M., Mishima, K., Saito, I., Okano, H., and Mizushima, N. 2006. Suppression of basal autophagy in neural cells causes neurodegenerative disease in mice. *Nature*, **441**: 885–889.

Harada, A., Takei, Y., Kanai, Y., Tanaka, Y., Nonaka, S., and Hirokawa, N. 1998. Golgi vesiculation and lysosome dispersion in cells lacking cytoplasmic dynein. *J. Cell Biol*., **141**: 51–59.

Heald, R., Tournebize, R., Blank, T., Sandaltzopoulos, R., Becker, P., Hyman, A., and Karsenti, E. 1996. Self-organization of microtubules into bipolar spindles around artificial chromosomes in Xenopus egg extracts. *Nature*, **382**: 420–425.

Hirose, H., Arasaki, K., Dohmae, N., Takio, K., Hatsuzawa, K., Nagahama, M., Tani, K., Yamamoto, A., Tohyama, M., and Tagaya, M. 2004. Implication of ZW10 in membrane trafficking between the endoplasmic reticulum and Golgi. *EMBO J*., **23**: 1267–1278.

Hollenbeck, P.J. 1993. Products of endocytosis and autophagy are retrieved from axons by regulated retrograde organelle transport. *J. Cell Biol*., **121**: 305–315.

Holzbaur, E.L., Hammarback, J.A., Paschal, B.M., Kravit, N.G., Pfister, K.K., and Vallee, R.B. 1991. Homology of a 150K cytoplasmic dynein-associated polypeptide with the Drosophila gene Glued. *Nature*, **351**: 579–583.

Ichimura, Y., Kirisako, T., Takao, T., Satomi, Y., Shimonishi, Y., Ishihara, N., Mizushima, N., Tanida, I., Kominami, E., Ohsumi, M., Noda, T., and Ohsumi, Y. 2000. A ubiquitin-like system mediates protein lipidation. *Nature*, **408**: 488–492.

Inoue, S. and Salmon, E.D. 1995. Force generation by microtubule assembly/disassembly in mitosis and related movements. *Mol. Biol. Cell*, **6**: 1619–1640.

Iwata, A., Riley, B.E., Johnston, J.A., and Kopito, R.R. 2005. HDAC6 and microtubules are required for autophagic degradation of aggregated huntingtin. *J. Biol. Chem*., **280**: 40282–40292.

Jahreiss, L., Menzies, F.M., and Rubinsztein, D.C. 2008. The itinerary of autophagosomes: From peripheral formation to kiss-and-run fusion with lysosomes. *Traffic*.

Jordens, I., Fernandez-Borja, M., Marsman, M., Dusseljee, S., Janssen, L., Calafat, J., Janssen, H., Wubbolts, R., and Neefjes, J. 2001. The Rab7 effector protein RILP controls lysosomal transport by inducing the recruitment of dynein-dynactin motors. *Curr. Biol*., **11**: 1680–1685.

Kabeya, Y., Mizushima, N., Ueno, T., Yamamoto, A., Kirisako, T., Noda, T., Kominami, E., Ohsumi, Y., and Yoshimori, T. 2000. LC3, a mammalian homologue of yeast Apg8p, is localized in autophagosome membranes after processing. *EMBO J*., **19**: 5720–5728.

Kamimoto, T., Shoji, S., Hidvegi, T., Mizushima, N., Umebayashi, K., Perlmutter, D.H., and Yoshimori, T. 2005. Intracellular inclusions containing mutant alpha 1-antitrypsin Z are propagated in the absence of autophagic activity. *J. Biol. Chem*., **281**: 4467–4476.

Kimura, S., Noda, T., and Yoshimori, T. 2007. Dissection of the autophagosome maturation process by a novel reporter protein, tandem fluorescent-tagged LC3. *Autophagy*, **3**: 452–460.

Kirisako, T., Baba, M., Ishihara, N., Miyazawa, K., Ohsumi, M., Yoshimori, T., Noda, T., and Ohsumi, Y. 1999. Formation process of autophagosome is traced with Apg8/Aut7p in yeast. *J. Cell Biol*., **147**: 435–446.

Klionsky, D.J. and Ohsumi, Y. 1999. Vacuolar import of proteins and organelles from the cytoplasm. *Annu. Rev. Cell Dev. Biol*., **15**: 1–32.

Kochl, R., Hu, X.-W., Chan, E.-Y. W., and Tooze, S.A. 2006. Microtubules facilitate autophagosome formation and fusion of autophagosomes with endosomes. *Traffic*, **7**: 1–17.

Komatsu, M., Waguri, S., Chiba, T., Murata, S., Iwata, J., Tanida, I., Ueno, T., Koike, M., Uchiyama, Y., Kominami, E., and Tanaka, K. 2006. Loss of autophagy in the central nervous system causes neurodegeneration in mice. *Nature*, **441**: 880–884.

Kouno, T., Mizuguchi, M., Tanida, I., Ueno, T., Kanematsu, T., Mori, Y., Shinoda, H., Hirata, M., Kominami, E., and Kawano, K. 2005. Solution structure of microtubule-associated protein light chain 3 and identification of its functional subdomains. *J. Biol. Chem*., **280**: 24610–24617.

Lakadamyali, M., Rust, M.J., Babcock, H.P., and Zhuang, X. 2003. Visualizing infection of individual influenza viruses. *Proc. Natl. Acad. Sci. USA*, **100**: 9280–9285.

Matteoni, R. and Kreis, T.E. 1987. Translocation and clustering of endosomes and lysosomes depends on microtubules. *J. Cell Biol*., **105**: 1253–1265.

Mizushima, N., Sugita, H., Yoshimori, T., and Ohsumi, Y. 1998. A new protein conjugation system in human. The counterpart of the yeast Apg12p conjugation system essential for autophagy. *J. Biol. Chem*., **273**: 33889–33892.

Mizushima, N., Yamamoto, A., Hatano, M., Kobayashi, Y., Kabeya, Y., Suzuki, K., Tokuhisa, T., Ohsumi, Y., and Yoshimori, T. 2001. Dissection of autophagosome formation using Apg5-deficient mouse embryonic stem cells. *J. Cell Biol*., **152**: 657–668.

Nakagawa, I., Amano, A., Mizushima, N., Yamamoto, A., Yamaguchi, H., Kamimoto, T., Nara, A., Funao, J., Nakata, M., Tsuda, K., Hamada, S., and Yoshimori, T. 2004. Autophagy defends cells against invading group A Streptococcus. *Science*, **306**: 1037–1040.

Nakatogawa, H., Ichimura, Y., and Ohsumi, Y. 2007. Atg8, a ubiquitin-like protein required for autophagosome formation, mediates membrane tethering and hemifusion. *Cell*, **130**: 165–178.

Nielsen, E., Severin, F., Backer, J.M., Hyman, A.A., and Zerial, M. 1999. Rab5 regulates motility of early endosomes on microtubules. *Nat. Cell Biol*., **1**: 376–382.

Noda, T., Kim, J., Huang, W.P., Baba, M.,Tokunaga, C., Ohsumi, Y., and Klionsky, D.J. 2000. Apg9p/Cvt7p is an integral membrane protein required for transport vesicle formation in the Cvt and autophagy pathways. *J. Cell Biol*., **148**: 465–480.

Ogawa, M., Yoshimori, T., Suzuki, T., Sagara., H., Mizushima, N., and Sasakawa, C. 2005. Escape of intracellular Shigella from autophagy. *Science*, **307**: 727–731.

Ravikumar, B., Acevedo-Arozena, A., Imarisio, S., Berger, Z., Vacher, C., O'Kane, C.J., Brown, S.D., and Rubinsztein, D.C. 2005. Dynein mutations impair autophagic clearance of aggregate-prone proteins. *Nat. Genet*., **37**: 771–776.

Ravikumar, B., Duden, R., and Rubinsztein, D.C. 2002. Aggregate-prone proteins with polyglutamine and polyalanine expansions are degraded by autophagy. *Hum. Mol. Genet*., **11**: 1107–1117.

Rubinsztein, D.C., Ravikumar, B., Acevedo-Arozena, A., Imarisio, S., O'Kane, C.J., and Brown, S.D. 2005. Dyneins, autophagy, aggregation and neurodegeneration. *Autophagy*, **1**: 177–178.

Schroer, T.A. and Sheetz, M.P. 1991. Two activators of microtubule-based vesicle transport. *J. Cell Biol*., **115**: 1309–1318.

Seglen, P.O. and Bohley, P. 1992. Autophagy and other vacuolar protein degradation mechanisms. *Experientia*, **48**: 158–172.

Sugawara, K., Suzuki, N.N., Fujioka, Y., Mizushima, N., Ohsumi, Y., and Inagaki, F. 2004. The crystal structure of microtubule-associated protein light chain 3, a mammalian homologue of Saccharomyces cerevisiae Atg8. *Genes Cells*, **9**: 611–618.

Suzuki, K., Kamada, Y., and Ohsumi, Y. 2002. Studies of cargo delivery to the vacuole mediated by autophagosomes in Saccharomyces cerevisiae.

Dev. Cell, **3**: 815–824.

Suzuki, K., Kubota, Y., Sekito, T., and Ohsumi, Y. 2007. Hierarchy of Atg proteins in pre-autophagosomal structure organization. *Genes Cells*, **12**: 209–218.

Tanida, I., Ueno, T., and Kominami, E. 2004. LC3 conjugation system in mammalian autophagy. *Int. J. Biochem. Cell Biol*., **36**: 2503–2518.

Webb, J.L., Ravikumar, B., and Rubinsztein, D.C. 2004. Microtubule disruption inhibits autophagosome-lysosome fusion: implications for studying the roles of aggresomes in polyglutamine diseases. *Int. J. Biochem. Cell Biol*., **36**: 2541–2550.

Yoshimori, T. 2004. Autophagy: a regulated bulk degradation process inside cells. *Biochem. Biophys. Res. Commun*., **313**: 453–458.

Yue, Z. 2007. Regulation of neuronal autophagy in axon: implication of autophagy in axonal function and dysfunction/degeneration. *Autophagy*, **3**: 139–141.

(Received for publication January 16, 2008 and accepted March 19, 2008)